Fernández Sáez, J.; El Ouardi, Y.; Bonastre Cano, JA.; Molina, JM.; Cases, F. (2019). Modification of the magnesium corrosion rate in physiological saline 0.9 wt % NaCl via chemical and electrochemical coating of reduced graphene oxide. Corrosion Science. 152:75-81. https://doi.org/10.1016/j.corsci.2019.01.025

Modification of the magnesium corrosion rate in physiological saline 0.9 wt % NaCl via chemical and electrochemical coating of reduced graphene oxide

J. Fernández [a], Y. El Ouardi [a], J. Bonastre [a], J.M. Molina [b], F. Cases [a, *]

[a] *Departamento de Ingeniería Textil y Papelera, Escuela Politécnica Superior de Alcoy, Universitat Politècnica de València, Plaza Ferrándiz y Carbonell, s/n, 03801 Alcoy, Spain.*

[b] *Departamento de Química Inorgánica de la Universidad de Alicante e Instituto Universitario de Materiales de Alicante, University of Alicante, Ap 99, E-03080 Alicante, Spain.*

Abstract

The synthesis of reduced graphene oxide onto magnesium discs by electrochemical and chemical methods is presented in this work. The surface morphology and atomic composition were investigated using field emission scanning electron microscopy and energy dispersive X-ray spectroscopy. The corrosion rate of different samples was analyzed in physiological saline 0.9 wt % NaCl solution by potentiodynamic polarization, electrochemical impedance spectroscopy and scanning electrochemical microscopy. As a result of the different treatments, a progressive decrease in the corrosion rate of the magnesium disc in the corroding environment was obtained, reaching up to 80% of reduction for the chemically modified sample.

Keywords: Magnesium; Reduced graphene oxide; Polarization curves; EIS; Corrosion

* Corresponding author. Tel.: +34 96 652 84 12; fax: +34 96 652 84 38.

E-mail address: fjcases@txp.upv.es (F. Cases).

1. Introduction

Different metallic materials have been used as biomaterials for the manufacture of medical implants. Commonly used metallic biomaterials include stainless steel, pure titanium, titanium-aluminum-vanadium-based alloys and cobalt-chromium-molybdenum-based alloys [1–5]. The advantages of biodegradable Mg-based implants [6–8] lie in their mechanical and electrochemical properties. Mg is a lightweight metal with a density of 1.74 g cm^{-3} versus 7.9 g cm^{-3} for Al and 4.5 g cm^{-3} for Ti. Moreover, Mg presents an elastic modulus and compressive yield strength closer to those of natural bone [9]. In addition, Mg is a biocompatible material naturally found in the human body (approximately half of the total physiological Mg is stored in the bone tissue) [10]. Setbacks when using Mg as metallic material for biomedical applications are related to its low corrosion resistance under the physiological conditions [9] and the excessively rapid production of hydrogen gas during the in-vivo corrosion [11]. The first issue could lead to both a rapid loss of its mechanical properties and severe problems in tissue regeneration, and the second, to harmful effects during the tissue healing process. One of the most recent studies dedicated to slowing down the dissolution of magnesium in saline conditions was performed on samples of magnesium foam manufactured using the replication method from carbon spheres as a template. The heat treatment in air flow at 540 ºC applied to burn the template particles generated a layer of oxide on the surface

of the foam which notably slowed down its dissolution at 37 °C in an aqueous solution containing 3 wt % NaCl that had a pH of 7.4 (a pH closed to that of the human body) [12]. Other surface modifications that were proved to be successful in slowing the corrosion rate of magnesium were fluoride conversion coatings, phosphate treatments or chemical deposition of hydroxyapatite and octacalcium phosphate [13].

Moreover, it has been proved that both graphene oxide (GO) and reduced graphene oxide (RGO) show anti-corrosion properties when coated onto metal substrates [14−19]. The syntheses of the different graphene-metallic substrate specimens were carried out following both electrochemical [20−22] and chemical [23,24] methods.

Accordingly, in the present research, the modification of the corrosion rate of a bare Mg-disc electrode by surface electrochemical/chemical coating of RGO from a GO solution in alkaline medium at pH = 11 is considered. During the chemical coating, bovine serum albumin (BSA) was coated onto the passivated Mg-surface to generate positive charges that enabled the anchoring of GO [25−28]. To observe the effect of the different treatments on the corrosion rate of Mg, the samples were analyzed in physiological saline 0.9 wt % NaCl solution (pH = 6.7) by impedance spectroscopy (EIS) and potentiodynamic polarization curves measurements. The surface electroactivity of different specimens at their open circuit potential (OCP) was recorded by scanning electrochemical microscopy (SECM). The microstructure and atomic composition were analyzed by field emission scanning electron spectroscopy (FESEM) and energy dispersive X-ray spectroscopy (EDX), respectively.

2. Experimental

2.1. Materials and samples

The original Mg samples were discs of 6 mm of diameter and 2 mm of thickness. The Mg discs were machined from an original rod of 7.9 mm in diameter purchased from GoodFellow Metals (Cambridge, United Kingdom). The chemical analysis reveals nominal major impurities (in ppm) of Fe (<280), Mn (<170), Al (<70) and Si (<50). A Pt thread was glued to one side of the disc with CircuitWorks® conductive epoxy resin. The resin was hardened at 85 ºC. Afterwards, the sample was sealed into a cone-tip cut from a 100-1000 µl Eppendorf® tip. The exposed area of the Mg electrode was successively ground with silicon carbide grinding paper of 320, 600 and 1200 grit, ultrasonicated in ethanol and dried at room temperature.

2.2. Electrochemical treatments

The electrochemical treatments carried out with a Mg electrode (M0) in an inert N_2 atmosphere are described as follows:

- Treatment (a); electrode E1: potentiostatic passivation in 6 M KOH solution at room temperature. A potential of -1.0 V vs. Ag/AgCl (KCl 3.0 M) was fixed for 30 minutes.
- Treatment (b); electrode E2: Mg electrode biased at -1.6 V vs. Ag/AgCl (KCl 3.0 M) for 30 minutes 0.1 M $LiClO_4$ (pH = 11) solution.
- Treatments (c and d); electrodes E3a and E3b: (c) potentiostatic synthesis of RGO at -1.6 V vs. Ag/AgCl (KCl 3.0 M) for 30 minutes or (d) 1 hour. Both syntheses were carried out in 3 g L^{-1} GO + 0.1 M $LiClO_4$ (pH = 11) solution. The value of pH was selected according to the research realized by Swarnima Kashyap et al. [29] to minimize the particle size of GO and to obtain a better dispersion of GO particles in the solution.

- Treatment (e); electrode E4: as in the treatment (c) but from a passivated electrode according to treatment (a).

2.3. Chemical treatments

The samples chemically modified were obtained according to these methods:

- Treatment (f); electrode Q1: A Mg electrode passivated in accordance with the treatment (a) was immersed in 0.5% (BSA) solution during 15 minutes and after being rinsed thoroughly with water, it was immersed for 30 minutes in the GO solution at pH = 11. Finally, the electrode was dried in an oven at 35 ºC and then reduced with dithionite in 50 mM $Na_2S_2O_4$ solution at 85 ºC for 30 minutes. The steps in the GO and dithionite solutions were repeated twice.
- Treatment (g); electrode Q2: The same than above, but in this case, the electrode was immersed in the GO and dithionite solutions four times.
- Treatment (h); electrode Q3: Directly from a bare Mg electrode and without the immersion in the BSA solution, the sample was treated in the GO and dithionite solutions four times.
- Treatment (i); electrode Q4: The same than in treatment (g) but without BSA.
- Treatment (j); electrode Q5: As in the treatment (g), but from a bare Mg electrode.

2.4. Electrochemical measurements

Electrochemical measurements in physiological saline (0.9 wt % NaCl at pH = 6.7) were carried out to research the effect of the different treatments on the corrosion resistance of bare Mg. The experiments were carried out in conventional three-electrode cell using a Ag/AgCl (KCl 3.0 M) reference electrode and a Pt thread (1 cm^2) as counter electrode. Tafel curves were recorded between -1.75 and -1.2 V at 1 mV s^{-1}. The electrochemical impedance spectroscopy (EIS) measurements ranged from 10^{-2} to 10^5

Hz. The amplitude of the sinusoidal voltage was ± 0.01 V from the OCP. The above measurements were recorded in an Autolab PGSTAT302 potentiostat/galvanostat. The SECM analyses were performed with a scanning electrochemical microscope of Sensolytics. The samples were mounted on microscope slices and immersed in 0.5 mM $Fe(CN)_6^{3-}$ + saline 0.9 wt % NaCl solution. Approach curves and SECM images were obtained with the samples unbiased, that is, at their OCP. All the SECM tests were carried out with a Pt microelectrode (10 μm diameter) at constant-height mode with the z-position of the electrode unchanged while scanning. The microelectrode was polarized at +0.4 V to detect the presence of $Fe(CN)_6^{4-}$ generated on the surface of the samples according to the scheme in Fig. 1.

2.5. FESEM and EDX analysis

The surface morphology and the elemental composition of the samples were measured with a Jeol JSM-6300 scanning electron microscope operating at a potential of 20 kV. EDX spectra were obtained between 0 and 20 keV.

3. Results and discussion

3.1. Electrochemically modified electrodes

In order to assign the potential ranges for the electrochemical processes occurring on the Mg-surface, different CV voltammograms have been recorded in the solutions in which the different electrochemical procedures (electrochemical synthesis of RGO and pretreatment of Mg samples for the chemical synthesis) were carried out. Fig. 2 shows the second CV scan obtained at a scan rate of 2.5 mV s^{-1} for a Mg electrode in (a) 6 M KOH and (b) 0.1 M $LiClO_4$ (pH = 11) solutions. As could be seen in Fig. 2a, the anodic sweep shows four processes that according to Lei et al [30] and Cai et al. [31] are: the

active dissolution of Mg (between -1.5 and -0.5 V) and the formation on the electrode surface of a $Mg(OH)_2$ layer once the concentration of Mg^{2+} reached its saturation, direct oxidation of Mg to $Mg(OH)_2$ in the range from -0.5 to 0.5 V, secondary oxidation of Mg to form MgO (from 0.5 to 1.0 V) and the transpassive process (between 1.0 and 1.5 V) overlapped with the oxygen evolution. In Fig. 2b, the scan towards positive potentials (between -1.7 and -1.3 V) shows the evolution of the current density towards positive values. From about -1.49 V, the current density takes positive values up to 742 μA cm^{-2} due to the corrosion of the electrode surface. The inset in Fig. 2b shows the third CV scan in which a significant loss in the positive values of current density is observed once the electrode surface became passivated. The curves of current density vs. time for the treatments (a), (b) and (c), which were described in the section 2.2, are shown in Fig. 3. The values of current density are coherent with those in the CV curves of Fig. 2 and, after about 300 s, show a very stable trend.

Figs. 4a and b show the effect of the electrochemical treatments on the corrosion rate of Mg in physiological saline 0.9 wt % NaCl by means of Tafel polarization curves and impedance Nyquist plots, respectively. Their electrochemical parameters, deduced from those experiences, are summarized in Table 1. To obtain these parameters, the research carried out by M. Curioni et al. [32] in which the impedance response is correlated to the corrosion rate by the "apparent" Stern-Geary coefficient (B) was taken into consideration. Accordingly, the corrosion current (icorr) was estimated by the equation $icorr = B/(Rcp+Rct)$ where Rct is the charge transfer resistance, Rcp is the corrosion product resistance and B = 253 mV. The term (Rcp+Rct) was calculated from the Nyquist plot measuring the diameter of the capacitive loop (cutting segment of the resistance Z' axe at low and high frequencies). Compared to the Mg electrode (M0), it can be observed, from the polarization curves (Fig. 4a), that the electrochemical activity

of modified electrodes E1, E3a, E3b and E4 changes since the corrosion potential (Ecorr) shifts in the positive direction. No difference between M0 and E2 sample was observed. The samples E3a, E3b show a similar value of Ecorr which may indicate that the increase of half an hour during the treatment (d) has no effect in terms of Ecorr. The Nyquist plots (Fig. 4b) and Table. 1 show a decrease in the values of corrosion current density (Icorr) and an increase of the term (Rcp+Rct) with the modification of the surfaces for E1, E3a, E3b and E4.

Figs. 5a-d show the FESEM micrographs of M0, E1, E2 and E3a electrodes. The morphology of the E1 shows a honeycomb-like structure due to the dissolution of magnesium and the formation of $Mg(OH)_2$ structures [21,33,34] during the treatment in 6 M KOH solution. The surface of E2 sample is characterized by interlocking plate-like structures of $Mg(OH)_2$ formed during the treatment in 0.1 M $LiClO_4$ (pH = 11) solution [21,33,34]. The surface of the E3a electrode appears much less modified than that of the E2 electrode due to the presence of GO during the electrosynthesis. This result is coherent with those reported by F. Wu et al. [21] in which the presence of GO into the solution of Mg^{2+} has a significant influence into deposition process and the microstructure of the coated GO-$Mg(OH)_2$ composite. In order to verify the nature of the coating, in Fig. 6 an EDX analysis for M0 and E3a electrodes was performed. An increase of about 5% in atomic carbon is observed for the E3a electrode (see Figs. 6a and b) due to the presence of RGO. In addition, the presence of oxygen increased mainly due to the formation of $Mg(OH)_2$ during the potentiostatic treatment in 3 g L^{-1} GO + 0.1 M $LiClO_4$ (pH = 11) solution.

3.2. Chemically modified electrodes

In the section 2.3, the procedures performed to coat RGO chemically on the Mg electrode surface were described. The different electrodes were named using the letter Q. As with the electrochemically modified electrodes, potentiodynamic polarization curves and EIS (Nyquist) plots were obtained in physiological saline 0.9 wt % NaCl (see Figs. 7a and b). Fitting results of the EIS measurements and the values of corrosion current density (Icorr) are summarized in Table 2. Compared to the results obtained for the electrochemical (E) samples, a shift towards more positive potentials is also observed. The Ecorr potential remains in both cases between -1.45 and -1.42 V. The values of Icorr are particular low for the samples Q1 and Q2. In comparison with the results for the sample Q4, it is noteworthy the role of BSA at neutralizing the negative charge on the passivated Mg and to promote the anchoring of GO to its surface. On the other hand, the result obtained for the sample Q5 would indicate that BSA acts on the passivated $Mg(OH)_2$ surface but not on the bare Mg surface. From the EIS spectra, the high increment of the (Rcp+Rct) term for the samples Q1, Q2 can be noted, and, to a lesser extent, for the sample Q4 which is passivated but has not undergone the treatment with BSA. From the potentiodynamic polarization curves in Fig. 7a, it is noticeable to observe that once the Ecorr potential is exceeded, the Icorr for the samples Q1, Q2, Q3 and Q4 takes negative values in the range up to -1.2 V which indicates a significant protection of Mg surface by the presence of RGO. Fig. 8 depicts the morphology of the RGO chemically synthesized on the Q2 sample and its EDX spectrum. The typical corrugated structure of RGO is clearly visible and by 47.2% of atomic carbon was measured. The average values of carbon atomic content (obtained from the EDX spectra recorded at different points on the surface of the samples) for Q2, Q3 and Q4 were 44.1%, 13.6% and 4.3%, respectively. The increase in the atomic percentage of carbon

for the sample Q2 is indicative of the effect of BSA at promoting the anchorage of GO onto the passivated Mg surface.

3.3. SECM analysis

Fig. 9a shows the z-approach towards the surface of different samples in 5 mM $Fe(CN)_6^{3-}$ and physiological saline 0.9 wt % NaCl solution with the microelectrode at +0.4 V. I and L are the normalized current tip and distance between microelectrode and sample, respectively. For a disc-shaped tip, the terms I and L are given by the equations [35]:

$I = i_T/i_{T,inf}$ where $i_{T,inf} = 4naFD_AC_A$, n is the number of electrons exchanged in the redox reaction, a is the radius of the microelectrode, F is the Faraday constant, D_A is the diffusion coefficient of A and C_A the concentration of A in the bulk solution.

$L = d/a$ where d is the separation between sample and microelectrode and a is the radius of the microelectrode.

A clear "positive feedback" [35] is observed for M0 sample which indicates a very active surface as a consequence of the Mg surface corrosion. The sample E2 also shows a "positive feedback" situation but to a lesser extent. It is for the passivated sample (according to treatment (a)) E1, and the samples with RGO (E3a and Q2) for which a significant loss of activity is observed. This fact indicates the protection of the surfaces from the corrosion but no a complete electrochemical isolation since a "negative feedback" was not observed. Figs. 9b-f show the electrochemical and chemical maps for M0, E1, E2, E3a and Q2 samples. In the 3D-Array image of M0 (see Fig. 9b), higher current values correspond to anodic zones with corrosion and lower current values mean lower activity. Therefore, the encircled area in the image of Fig. 9b suggests a pit corrosion zone on the Mg surface [36]. In Fig. 9c, the SECM image for E1 sample is

homogeneous and featureless, which reveals that the treatment (a) creates a passivated surface with higher corrosion resistance. Fig. 9d shows the array scan for the sample E2, in this case the surface shows the characteristic of M0 but with lesser intensity. The E3a sample shows better corrosion resistance than E2 but the SECM image is not so homogeneous as E1. That is, E3a surface is more active than this for E1. Finally, the SECM image for Q2 recovers the characteristics of E1 sample showing a very low activity during the time (about 1 hour) that takes to obtain of the line scans and 3D-maps.

4. Conclusions

The electrochemical properties of a bare Mg surface have been successfully modified by electrochemical and chemical methods. The best results were obtained with the chemical treatment for Q2 sample. BSA improves the anchoring of GO on the Mg passivated surface by the neutralization of the negative charges. The corrosion rate was modulated progressively between 1.13 and 0.21 mA cm^{-2} which would allow the choice of a certain sample depending on the requirements of the biomedical application. SECM images confirm the increment of the corrosion resistance of the samples coated with RGO.

Acknowledgment

The authors wish to thank the Spanish Agencia Estatal de Investigación (AEI) and European Union (FEDER funds) for the financial support (contracts MAT2016-77742-C2-1-P and MAT2016-77742-C2-2-P). Tim Vickers is gratefully acknowledged for help with the English revision. Electron Microscopy Service of the UPV (Universitat

Politècnica de València) is gratefully acknowledged for help with FESEM and EDX characterization.

Data availability

The processed data required to reproduce these findings are available to download from [https://data.mendeley.com/datasets/cfsfb28zzn/2].

References

[1] U. Zwicker, K. Buhler, R. Muller, H. Beck, H.J. Schmid, J. Ferstl, Mechanical Properties and Tissue Reactions of a Titanium Alloy for Implant Material. In Titanium'80, Science and Technology; Kimura, I., Ed.; Metallurgical Society of AIME: New York, NY, USA, 1980 Volume 1, pp. 505–514.

[2] B.P. Bannon, E.E. Mild, Titanium Alloys for Biomaterial Application: An Overview. Titanium Alloys in Surgical Implants; ASTM: Philadelphia, PA, USA, 1983, pp. 7–15.

[3] M. Long, H.J. Rack, Titanium alloys in total joint replacement −A materials science perspective, Biomaterials 19 (1998) 1621–1639.

[4] M. Niinomi, Recent metallic materials for biomedical applications, Metall. Mater. Trans. A 33 (2002) 477–486.

[5] T. Hanawa, Recent development of new alloys for biomedical use. Mater. Sci. Forum 512 (2006) 243–248.

[6] F. White, The history of biodegradable magnesium implants: A review, Acta Biomaterialia 6 (2010) 1680–1692.

[7] H. Waizy, J.M. Seitz, J. Reifenrath et al., Biodegradable magnesium implants for orthopedic applications, J. Mater. Sci. 48 (2013) 39–50.

[8] K. Kumar, R.S. Gill, U. Batra, Challenges and opportunities for biodegradable magnesium alloy implants, Materials Technology 33 (2017) 153−172.

[9] M.P. Staiger, A.M. Pietak, J. Huadmai, G. Dias, Magnesium and its alloys as orthopedic biomaterials: A review, Biomaterials 27 (2006) 1728−1734.

[10] Merck Manual of Diagnosis and Therapy (online): Section 2: Endocrine & metabolic disorders, chapter 12: Water, electrolyte, mineral, and acid-base metabolism, seventeenth ed.

[11] F. Witte, V. Kaese, H. Haferkamp, E Switzer, A. Meyer-Lindenberg, C.J. Wirth, et al., In vivo corrosion of four magnesium alloys and the associated bone response, Biomaterials 26 (2005) 3557–3563.

[12] J.M. Ferri, J.M. Molina, E. Louis, Fabrication of Mg foams for biomedical applications by means of a replica method based upon spherical carbon particles, Biomedical Physics & Engineering Express 1 (2015) 045002.

[13] T.S.N. Sankara, I.S. Park, M.H. Lee (Eds.), Surface modification of magnesium and its alloys for biomedical applications, Woodhead Publishing (2015).

[14] N.T. Kirkland, T. Schiller, N. Medhekar, N. Birbilis, Exploring graphene as a corrosion protection barrier, Corros. Sci. 56 (2012) 1–4.

[15] B.P. Singh, S. Nayak, K.K. Nanda, B.K. Jena, S. Bhattacharjee, Laxmidhar Besra, The production of a corrosion resistant graphene reinforced composite coating on copper by electrophoretic deposition, Carbon 61 (2013) 47–56.

[16] B. Ramezanzadeh, A. Ahmadi, M. Mahdavian, Enhancement of the corrosion protection performance and cathodic delamination resistance of epoxy coating through treatment of steel substrate by a novel nanometric sol-gel based silane composite film filled with functionalized graphene oxide nanosheets, Corros. Sci. 109 (2016) 182–205.

[17] K. Qi, Y. Sun, H. Duan, X. Guo, A corrosion-protective coating based on a solution-processable polymer-grafted graphene oxide nanocomposite, Corros. Sci. 98 (2015) 500–506.

[18] B. Ramezanzadeh, S. Niroumandrad, A. Ahmadi, M. Mahdavian, M.H. Mohamadzadeh Moghadam, Enhancement of barrier and corrosion protection performance of an epoxy coating through wet transfer of amino functionalized graphene oxide, Corros. Sci. 103 (2016) 283–304.

[19] Z. Yang, W. Sun, L. Wang, S. Li, T. Zhu, G. Liu, Liquid-phase exfoliated fluorographene as a two dimensional coating filler for enhanced corrosion protection performance, Corros. Sci. 103 (2016) 312–318.

[20] J. Zhao, X. Xie, Ch. Zhang, Effect of the graphene oxide additive on the corrosion resistance of the plasma electrolytic oxidation coating of the AZ31 magnesium alloy, Corros. Sci. 114 (2017) 146–155.

[21] F. Wu, J. Liang, W. Li, Electrochemical deposition of $Mg(OH)_2$/GO composite films for corrosion protection of magnesium alloys, J. Magnesium Alloys 3 (2015) 231–236.

[22] X.Z. Deng, Y.W. Wang, J.P. Peng, K.J. Liu, N.X. Feng, Y.Z. Di, Surface area control of nanocomposites $Mg(OH)_2$/graphene using cathodic electrodeposition process: high adsorption capability of methyl orange, RSC Adv. 6 (2016) 88315–88320.

[23] M. Heidarizad, S.S. Sengör, Synthesis of graphene oxide/magnesium oxide nanocomposites with high-rate adsorption of methylene blue, J. Mol. Liq. 224 (2016) 607–612.

[24] L. Baojun, H. Cao, G. Yin, $Mg(OH)_2$@reduced Graphene oxide composite for removal of dyes from water, J. Mater. Chem. 21 (2011) 13765–13768.

[25] Y.J. Yun, W.G. Hong, W-J. Kim, Y. Jun, B.H. Kim, A novel method for applying reduced graphene oxide directly to electronic textiles from yarns to fabrics, Adv. Mater. 25 (2013) 5701–5705.

[26] J. Molina, J. Fernández, M. Fernandes, A.P. Souto, M.F. Esteves, J. Bonastre, F. Cases, Plasma treatment of polyester fabrics to increase the adhesion of reduced Graphene oxide, Synth. Met. 202 (2015) 110–122.

[27] P. Yang, Q. Liu, J. Liu, H. Zhang, Z. Li, R. Li, L. Liu, J. Wang, Bovine serum albumin-coated graphene oxide for effective adsorption of uranium (VI) from aqueous solutions, Ind. Eng. Chem. Res. 56 (2017) 3588–3598.

[28] C. Wang, R. Guo, Sh. Lin, J. Lan, Sh. Jiang, Ch. Xiang, A highly electro-conductive and flexible fabric functionalized with bovine serum albumin for wearable electronic device, J. Mater. Sci. Mater. Electron. 29 (2018) 14927–14934.

[29] S. Kashyap, Sh. Mishra, Sh.K. Behera, Aqueous colloidal of graphene oxide and chemically converted graphene, J. Nanoparticles 2014 (2014) 1–6.

[30] T. Lei, Ch. Ouyang, W. Tang, L-F. Li, L-Sh. Zhou, Preparation of MgO coatings on magnesium alloys for corrosion protection, Surf. Coat. Technol. 204 (2010) 3798–3803.

[31] Z. Cai, D. Lu, W.li, Y. Liang, H. Zhou, Study on anodic oxidation of magnesium in 6 M KOH solution by alternative current impedance, Int. J. Hydrogen Energy 34 (2009) 467–472.

[32] M. Curioni, F. Scenini, T. Monetta, F. Bellucci, Correlation between electrochemical impedance measurements and corrosion rate of magnesium investigated by real-time hydrogen measurement and optical imaging, Electrochim. Acta 166 (2015) 372–384.

[33] M.A. Shah, F.M. Al-Marzouki, A simple and safe method for preparation of $Mg(OH)_2$ nanorods in ambient air, Int. J. Nano Dim. 2 (2011) 111–116.

[34] G. Balducci, L.B. Diaz, D.H. Gregory, Recent progress in the synthesis of nanostructured magnesium hydroxide, Cryst. Eng. Comm.19 (2017) 6067–6084.

[35] H. Xiong, J. Guo, Sh. Amemiya, Probing electron transfer at an unbiased conductor by scanning electrochemical microscopy in the feedback mode, Anal. Chem. 79 (2006) 2735–2744.

[36] X. Liu, T. Zhang, Y. Shao, G. Meng, F. Wang, Effect of alternating voltage treatment on the corrosion resistance of pure magnesium, Corr. Sci. 15 (2009) 1772–1779.

Figure Captions

Fig. 1. Scheme of the SECM tip collection/substrate generation mode for a Mg corroding surface.

Fig. 2. CV second scans for a Mg electrode in (a) 6 M KOH solution at 2.5 mV s^{-1} and (b) 0.1 M $LiClO_4$ (pH = 11) solution at 10 mV s^{-1}. The inset in Fig. 1b shows the third CV scan.

Fig. 3. Curves for the electrochemical treatments: (a) potentiostatic passivation in 6 M KOH at -1.0 V for 30 minutes, (b) Mg electrode at -1.6 V for 30 minutes in 0.1 M LiClO4 (pH=11) solution and (c) potentiostatic synthesis on a Mg electrode of RGO at -1.6 V for 30 minutes in 3 g L^{-1} GO + 0.1 M LiClO4 (pH = 11) solution.

Fig. 4. (a) Potentiodynamic polarization curves at a scan rate of 1 mV s^{-1} and (b) Nyquist plots recorded in the frequency range from 10^5 to 10^{-2} Hz for bare Mg and electrochemically modified electrodes in physiological saline 0.9 wt % NaCl. The frequencies values f1 and f2 were obtained for –Z" maximum and –Z" = 0, respectively.

Fig. 5. FESEM micrographs of samples (a) M0 (bare Mg), (b) E1, (c) E2 and (d) E3a. The micrographs were obtained at a magnification of 15.00 Kx.

Fig. 6. EDX spectra of samples M0 and E3a.

Fig. 7. (a) Potentiodynamic polarization curves obtained at a scan rate of 1 mV s^{-1} and (b) Nyquist plots recorded at the frequency range from 10^5 to 10^{-2} Hz for bare Mg and chemically modified samples in physiological saline 0.9 wt % NaCl. The frequencies values f1 and f2 were obtained for –Z" maximum and –Z" = 0, respectively.

Fig. 8. Magnified micrograph (Mag. = 15.00 Kx) of the structure of chemically synthetized RGO on Q2 sample and its EDX analysis.

Fig. 9. (a) Approach curves obtained with a Pt microelectrode (diameter 10 μm) at +0.4 V in 0.5 mM $Fe(CN)_6^{3-}$ + saline solution. The approach curves were recorded at an approach rate of 10 μm s^{-1}. (b-f) SECM images of M0, E1, E2, E3a and Q2 samples. The arrays were obtained at a scan rate of 20 μm s^{-1} and $\Delta x = \Delta y = 10$ μm.

Tables

Table. 1. Fitting results for the EIS measurements and corrosion current densities obtained in physiological saline 0.9 wt % NaCl for the samples electrochemically modified.

	Ecorr (V)	Icorr (mA cm^{-2})	Rcp+Rct (Ω cm^2)	Treatment
M0	**-1.52**	**1.13**	**223.0**	**Ø**
E1	**-1.43**	**0.82**	**308.4**	**a**
E2	**-1.53**	**1.15**	**219.6**	**b**
E3a	**-1.45**	**1.01**	**238.5**	**c**
E3b	**-1.45**	**0.93**	**271.4**	**d**
E4	**-1.47**	**1.06**	**250.7**	**e**

Table. 2. Fitting results for the EIS measurements and corrosion current densities obtained in physiological saline 0.9 wt % NaCl for the samples chemically synthesized.

	Ecorr (V)	Icorr (mA cm^{-2})	Rcp+Rct (Ω cm^2)	Treatment
M0	**-1.52**	**1.13**	**223.0**	**Ø**
Q1	**-1.42**	**0.29**	**861.9**	**f**
Q2	**-1.44**	**0.21**	**1213.1**	**g**
Q3	**-1.42**	**1.29**	**195.9**	**h**
Q4	**-1.45**	**0.76**	**331.9**	**i**
Q5	**-1.41**	**3.44**	**73.5**	**j**

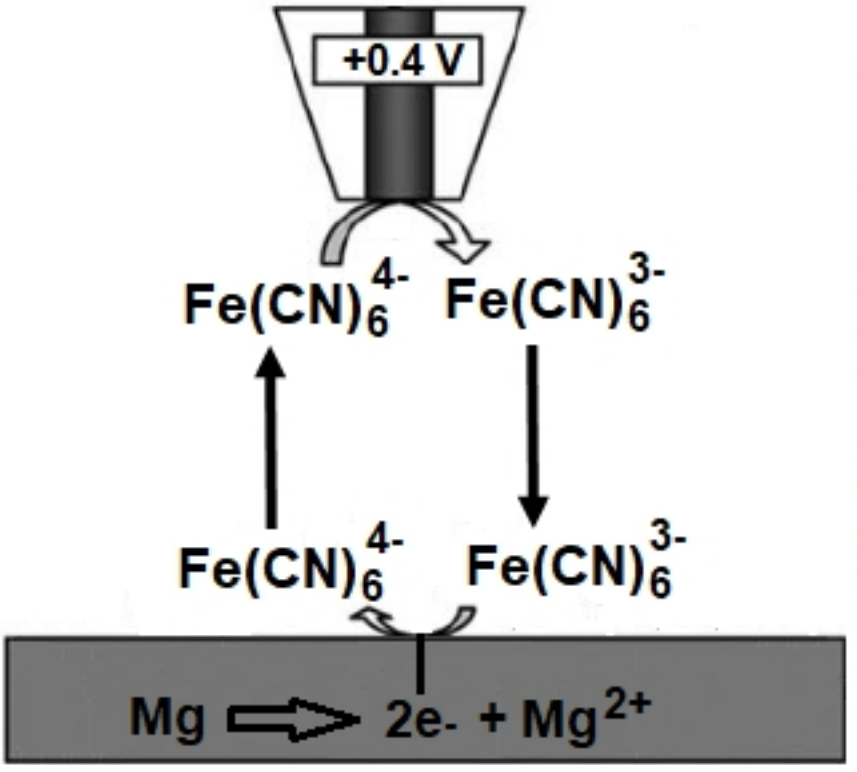
+0.4 V
Fe(CN)6 4-
Fe(CN)6 3-
Fe(CN)6 4-
Fe(CN)6 3-
Mg
2e-
+ Mg2+

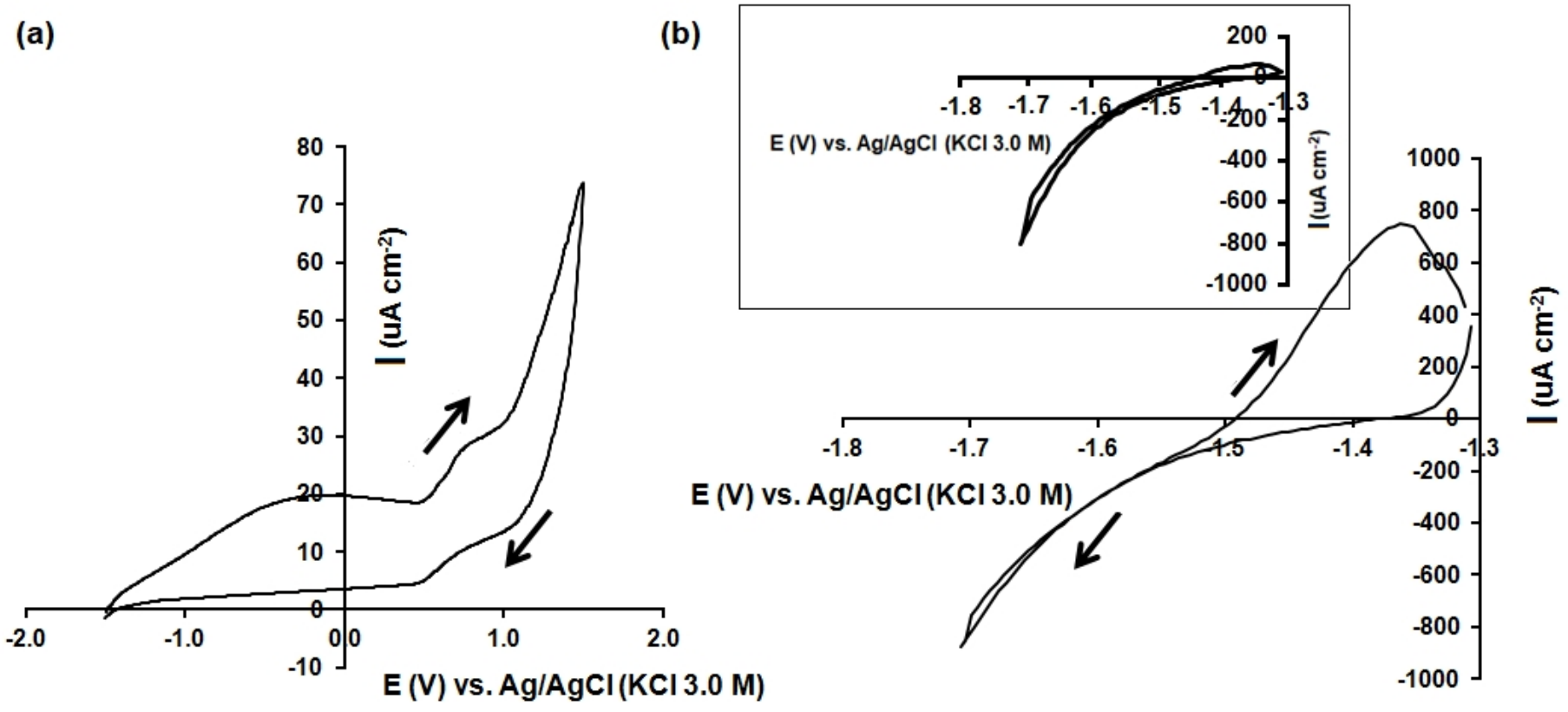
(a)
80
70
60
50
40
30
20
10
0
-10
-2.0
-1.0
0.0
1.0
2.0
I (uA cm-2)
E (V) vs. Ag/AgCl (KCl 3.0 M)
(b)
200
0
-200
-400
-600
-800
-1000
-1.8
-1.7
-1.6
-1.5
-1.4
-1.3
E (V) vs. Ag/AgCl (KCl 3.0 M)
I (uA cm-2)
1000
800
600
400
200
0
-200
-400
-600
-800
-1000
-1.8
-1.7
-1.6
-1.5
-1.4
-1.3
E (V) vs. Ag/AgCl (KCl 3.0 M)
I (uA cm-2)

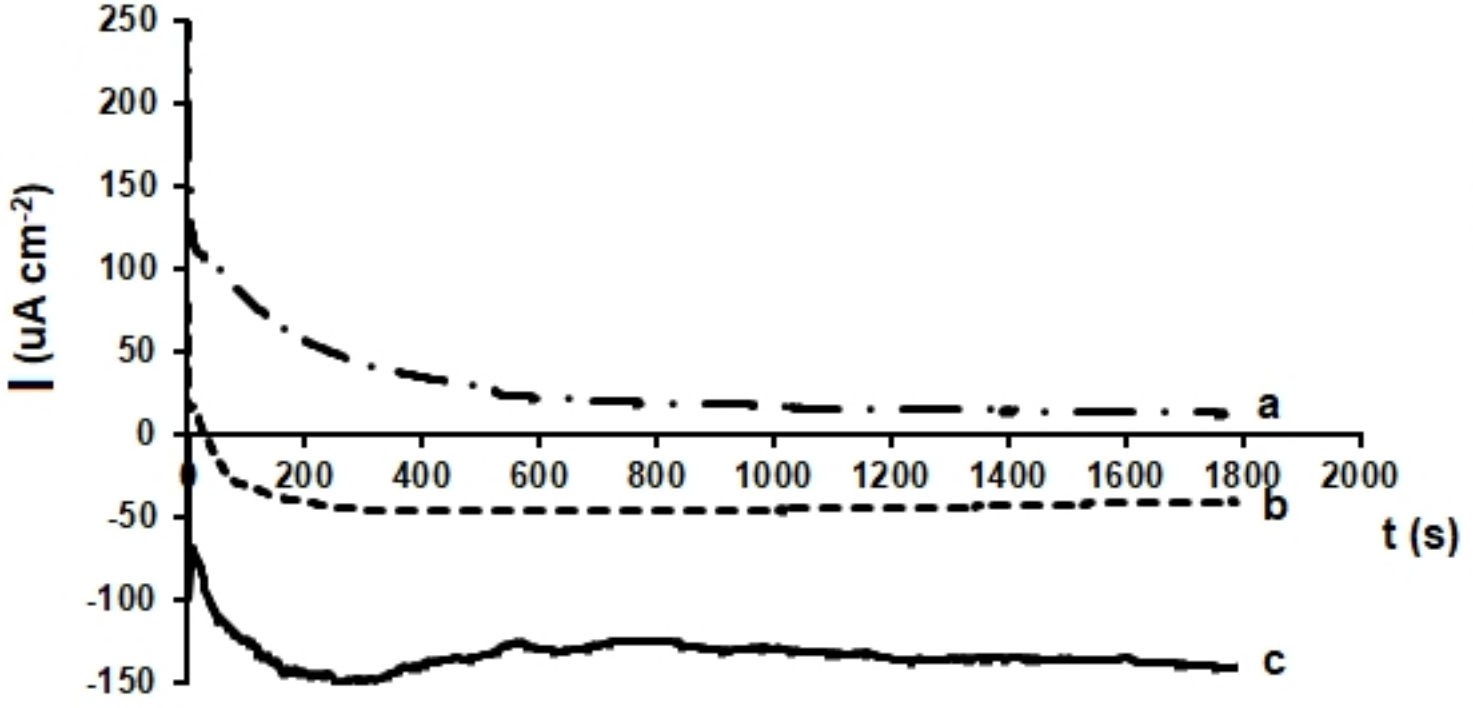
250
200
150
100
50
0
-50
-100
-150
I (uA cm-2)
200
400
600
800
1000
1200
1400
1600
1800
2000
t (s)
a
b
c

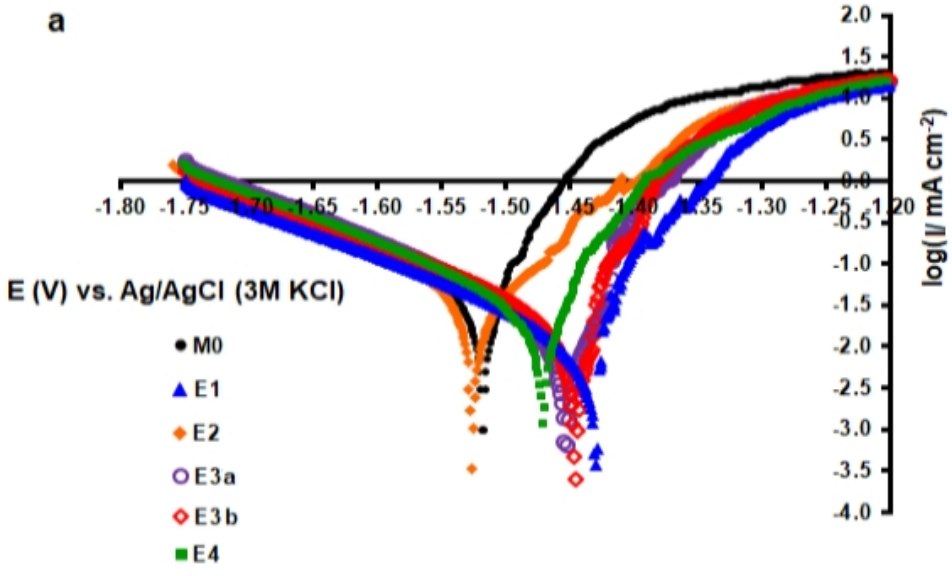

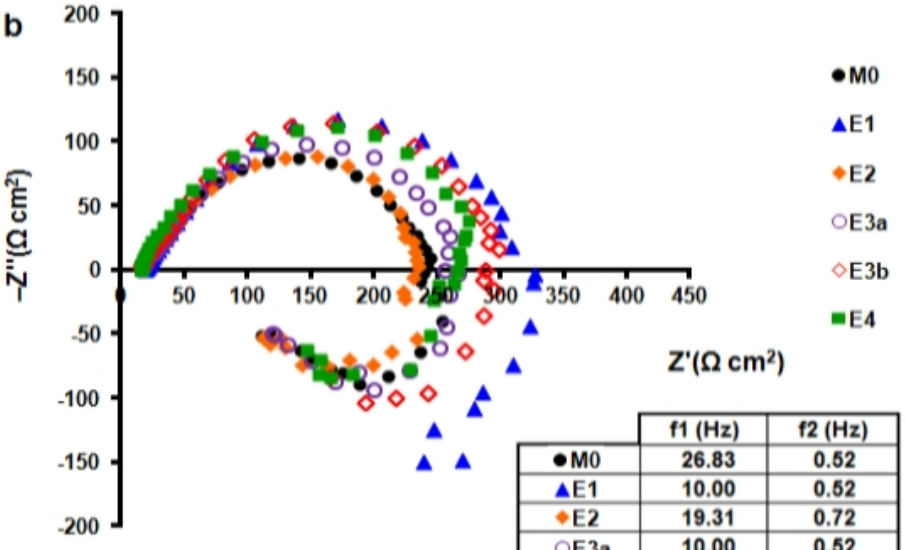

	f1 (Hz)	f2 (Hz)
M0	26.83	0.52
E1	10.00	0.52
E2	19.31	0.72
E3a	10.00	0.52
E3b	13.90	0.52
E4	26.83	0.72

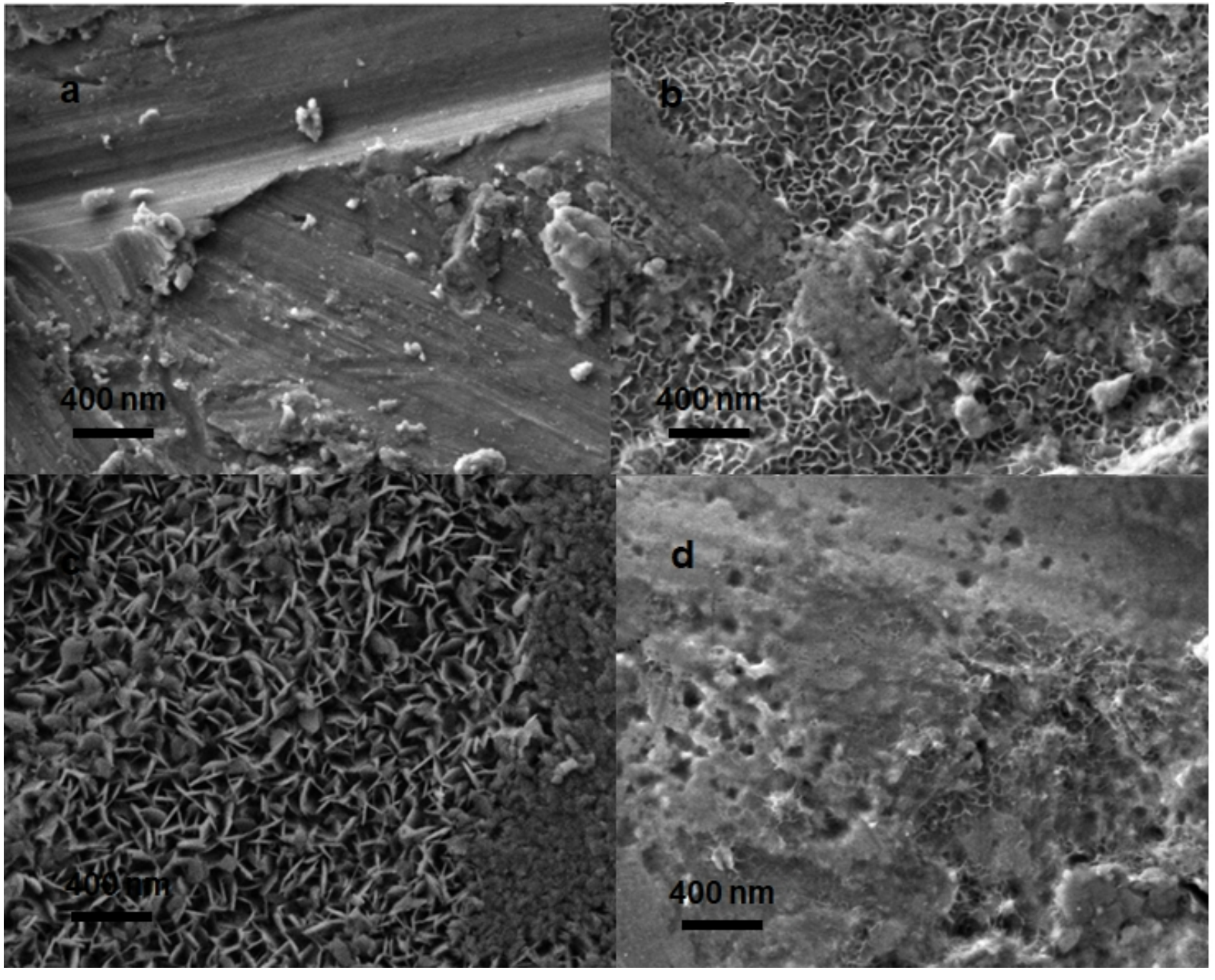
a
400 nm
b
400 nm
c
400 nm
d
400 nm

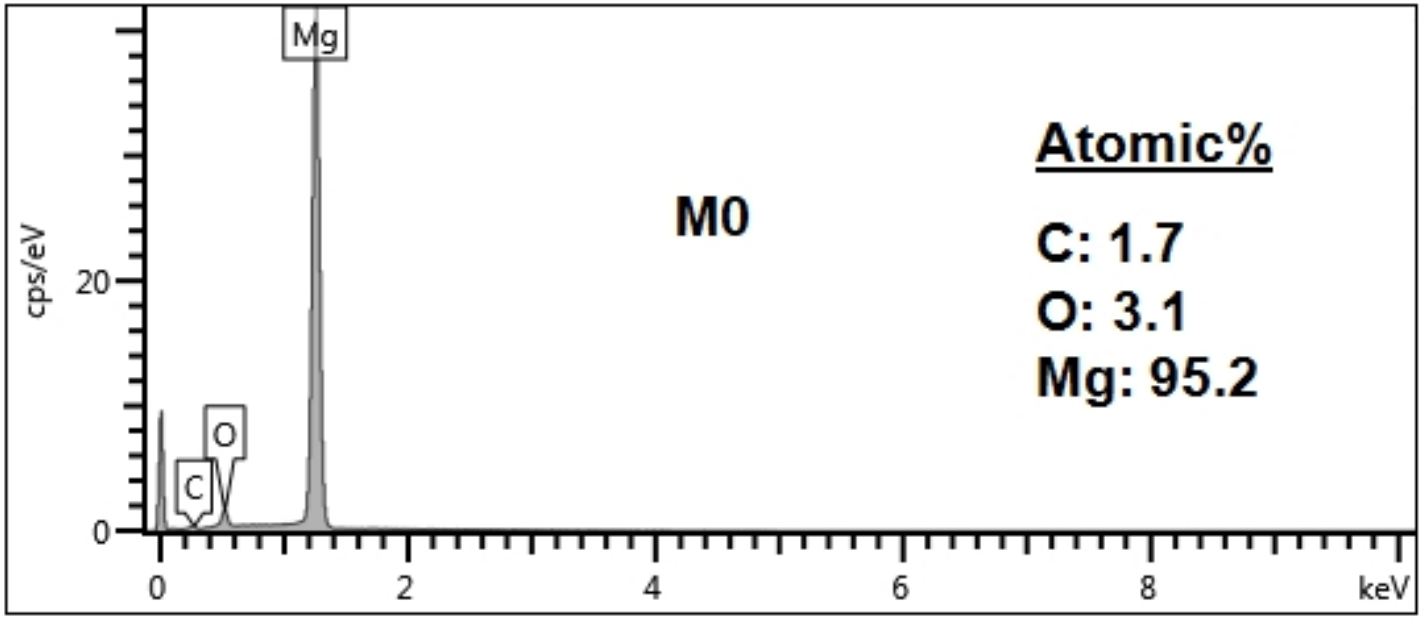
Mg
O
C
cps/eV
20
0
0
2
4
6
8
keV
M0
Atomic%
C: 1.7
O: 3.1
Mg: 95.2

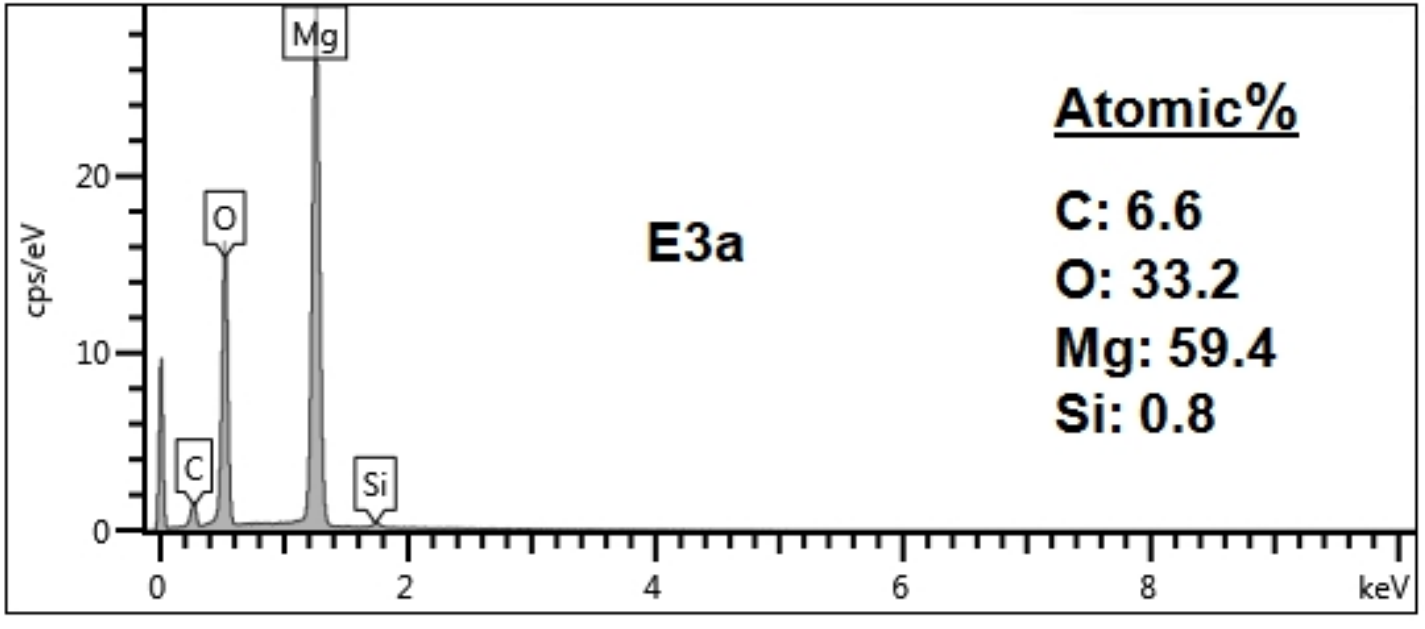
Mg
O
C
Si
cps/eV
20
10
0
0
2
4
6
8
keV
E3a
Atomic%
C: 6.6
O: 33.2
Mg: 59.4
Si: 0.8

a

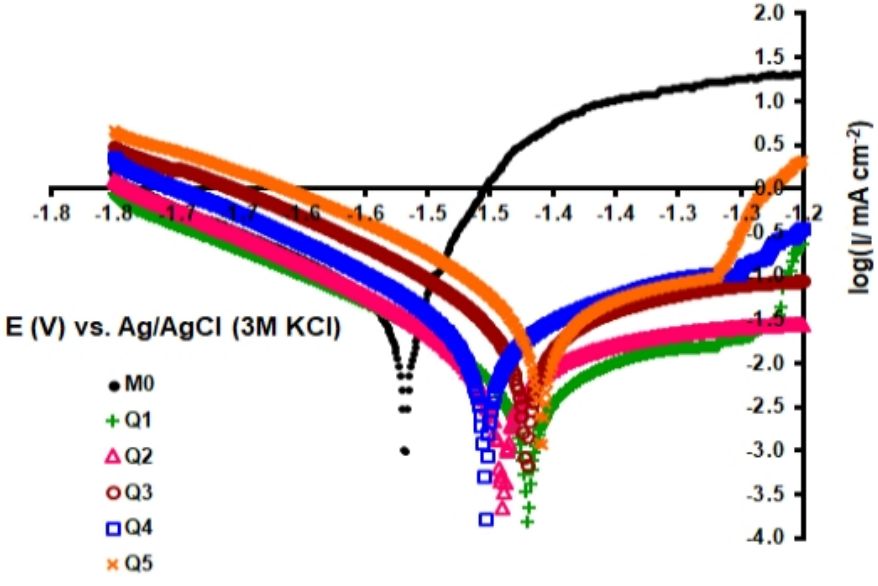

b

	f1 (Hz)	f2 (Hz)
M0	26.83	0.52
Q1	10.00	0.27
Q2	10.00	0.14
Q3	71.97	0.27
Q4	37.28	0.72
Q5	193.00	1.00

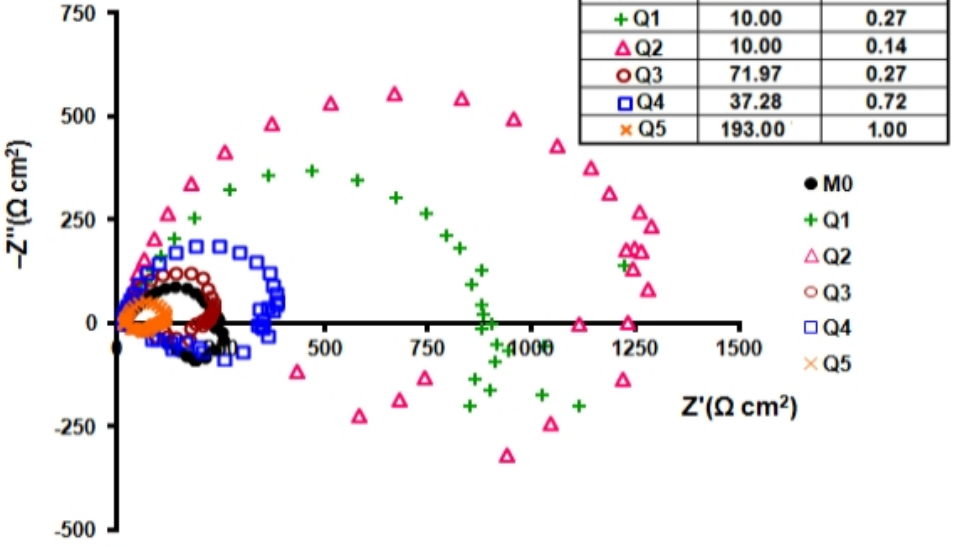

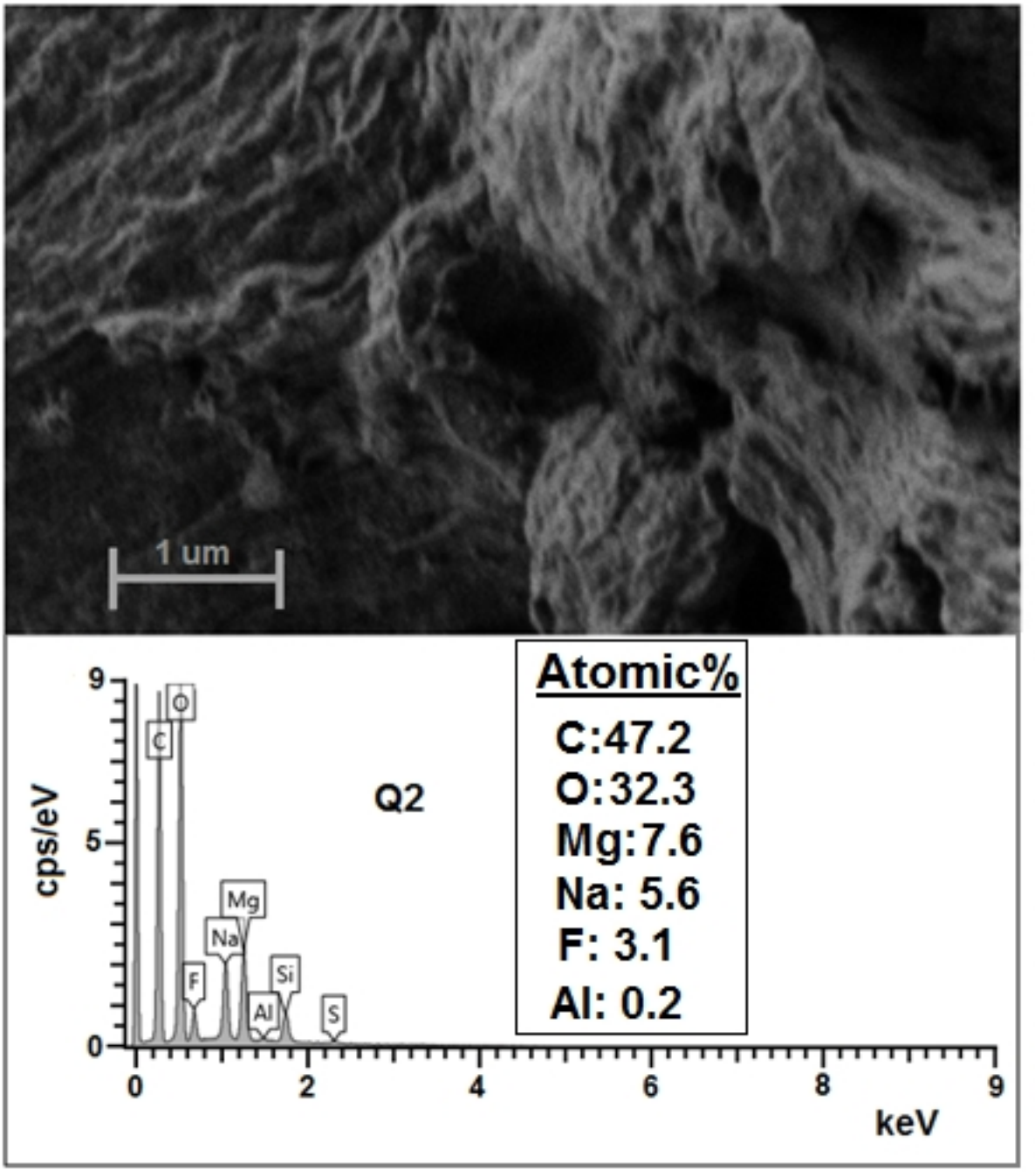
1 um
cps/eV
9
5
0
C
O
F
Na
Mg
Al
Si
S
Q2
0
2
4
6
8
9
keV
Atomic%
C:47.2
O:32.3
Mg:7.6
Na: 5.6
F: 3.1
Al: 0.2

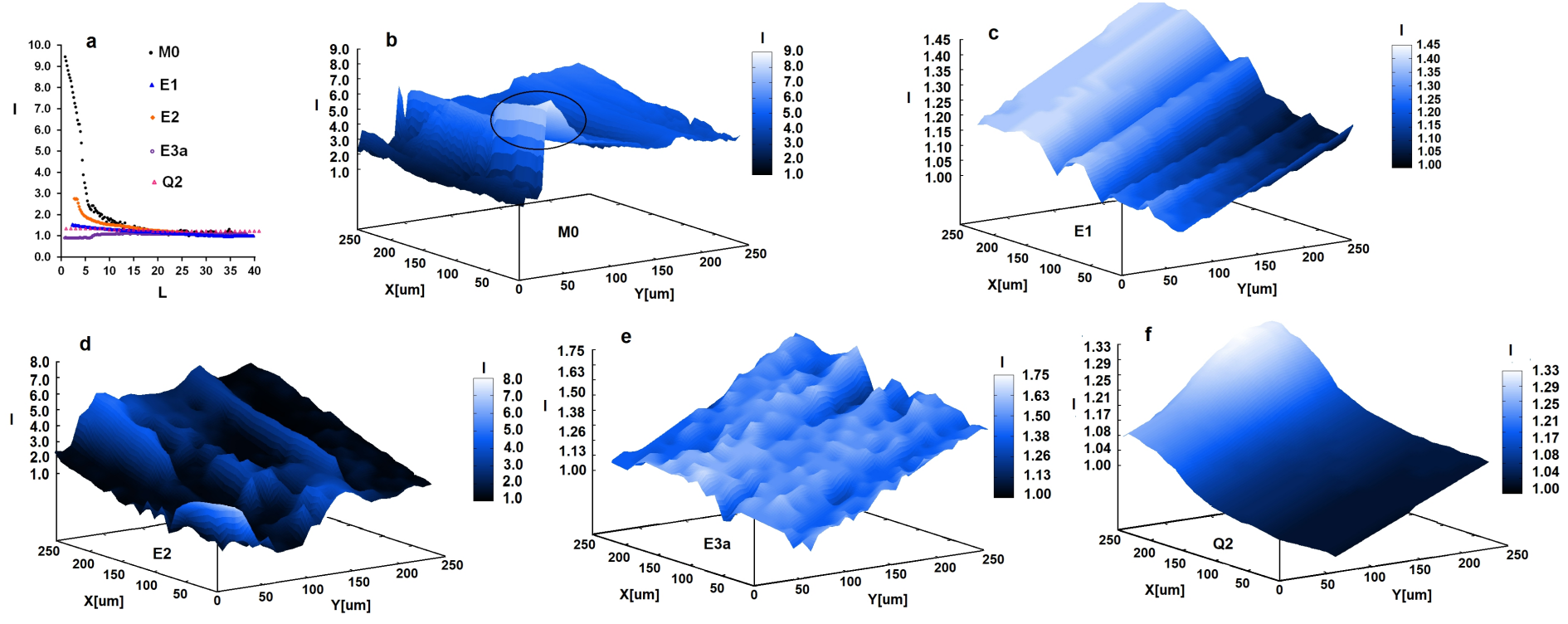
a
M0
E1
E2
E3a
Q2
I
L
b
M0
X[um]
Y[um]
c
E1
d
E2
e
E3a
f
Q2